# FAILURE OF ZIRCALOY-4 SHEET CONTAINING HYDRIDE BLISTERS

O.N. Pierron[1], D.A. Koss[1], A.T. Motta[2], R.S. Daum[3], and K.S. Chan[4]
[1]Dept. Materials Science and Engineering, Penn State Univ., University Park, PA 16802
[2]Dept. Mechanical and Nuclear Engineering, Penn State University, University Park, PA 16802
[3]Argonne National Laboratory, Argonne, IL 60439
[4]Southwest Research Institute, San Antonio, TX
[Corresponding Author: Donald Koss, 202A Steidle Bdg., Penn State University, University Park, PA 16802, koss@ems.psu.edu, phone: 814 865 5447, Fax: 814 865 2917]

## ABSTRACT

We have investigated the fracture behavior of unirradiated Zircaloy-4 sheet (0.64 mm thick) containing either model hydride blisters or a continuous hydrided layer "rim" at both 25° and 300°C and subject to the multi-axial stress state of near plane-strain tension. The blisters (either 2 or 3 mm in diameter) behave in a brittle manner, and the overall failure of the Zircaloy is controlled by fracture of the remaining "substrate" material. As a result, the fracture of the sheet is sensitive to the depth of the hydride layer/blister such that there is a significant decrease in ductility as the blister depth increases, up to a depth of about 100 μm. Beyond this value the ductility remains approximately constant. Importantly, moderate ductility is retained in the Zircaloy at 300°C for blisters of depths > 200 μm, even though such blister depths severely limit room temperature ductility. In general, the ductility of a material with a continuous hydride rim is less than that of a material containing blisters of the same depth. Experimental evidence as well as analytical modeling indicates that, while substrate fracture is controlled by crack growth at 25°C, the inhibition of crack growth at $300^0$C results in eventual failure due to an onset of a shear instability process. As a result, the Zircaloy remains relatively "tolerant" of isolated hydride blisters at 300°C.

## 1. INTRODUCTION

The mechanical behavior of Zircaloy fuel cladding degrades during nuclear reactor operation due to a combination of oxidation, hydriding, and radiation damage [1]. As the cladding undergoes oxidation with the associated hydrogen pickup, the total amount of hydrogen increases, and hydride precipitates form preferentially near the outer (cooler) surface of the cladding, usually in the form of a continuous layer/rim containing a high concentration of discrete hydrided particles. Under conditions where oxide spallation occurs, hydride *blisters* may form. The blisters are often lens shaped (typically a few mm in major dimension) and consist of a very high hydride concentration and/or a solid hydride [2].

The influence of a *uniform* distribution of hydrides on the mechanical behavior of zirconium-based alloys has been studied extensively, usually under uniaxial tensile loading; see for

example refs.[2-12]. Recent studies have also examined the failure behavior of Zircaloy-4 cladding tubes for the case when hydrides are present in the form of a layer or rim [13]. These "hydride-rim" results, based on unirradiated cladding, indicate a significant loss of ductility with increasing hydrogen content and/or increasing hydride rim thicknesses [13] and suggest that a ductile-to-brittle transition occurs with increasing hydride rim thickness.

In addition to the presence of hydrides, a second condition that affects cladding failure is the stress state associated with in-service loading. For the case of recrystallized zirconium alloy sheet containing a uniform distribution of hydrides, increasing the biaxiality of the stress state increases the severity of the hydrogen embrittlement [14]. Such an effect becomes an issue for Zircaloy cladding subject to postulated reactor accidents such as the reactivity-initiated accident (RIA) [15]. In this case, the interaction between fuel pellets and the cladding tubes forces the cladding to deform under multiaxial stress states. Predicting a criterion for cladding failure thus requires a knowledge of the influence of the effects of irradiation, the specific hydride microstructure, and the stress state of loading. This study addresses the latter two issues.

The purpose of this study is to examine the influence of *hydride blisters* on failure behavior of unirradiated Zircaloy-4 under the multiaxial stress state associated with near-plane strain deformation. Our approach ius to create a model system in which the effects of blisters on ductility can be studied separate from other parameters. Using a gas-charging procedure we introduced blisters of controlled depths in double notch tensile specimens that were specially designed to create biaxial tension and near plane-strain tension deformation within the gauge section . To study the influence of blisters it is necessary to have a gauge section that is large compared to the blister diameter (2-3 mm). Because of this we utilize flat Zircaloy-4 sheet with a crystallographic texture (and plastic anisotropy) similar to that of as-fabricated Zircaloy-4 cladding tubes. Both cold worked and stress-relieved as well as recrystallized conditions of the sheet are examined.

## 2. EXPERIMENTAL PROCEDURE

### 2.1 Materials Used

Zircaloy-4 sheet with a thickness of 0.64 mm was obtained from Teledyne Wah-Chang in the cold-worked, stress-relieved state (CWSR). Recrystallized (RX) material was obtained after annealing the as-received material at 650°C for 30 minutes in a vacuum of $10^{-5}$ Torr. The grain structure of the CWSR material, determined using polarized light microscopy, consisted of elongated grains, approximately 10 μm long and roughly 1-2 μm thick in the CWSR condition while equiaxed grains approximately 5 μm grain in diameter in were observed the RX condition.

Both the CWSR and RX conditions exhibited a strong crystallographic texture. The Kearns factors (resolved fraction of basal poles aligned with the three macroscopic directions, N=normal, L=longitudinal (rolling direction), T=transverse) [16], and measured by Teledyne Wah-Chang are shown in Table 1. The majority of the basal poles are aligned with the normal direction. Importantly, these values are similar to those reported for unirradiated CWSR Zircaloy-4 cladding tubes [17] if the hoop direction of the tube corresponds to the orientation transverse to the rolling direction of the sheet. Therefore, the texture of the sheets of Zircaloy-4 used in this study is similar to the typical texture of Zircaloy-4 cladding tubes, for which the basal planes tend to align with their poles inclined approximately ± 30º away from the normal of the tube surface and oriented towards the transverse direction [18].

Table 1. Kearns factors for both CWSR and RX Zircaloy-4 sheet and tubing.

| | $f_N$ | $f_L$ | $f_T$ |
|---|---|---|---|
| CWSR sheet (this work) | 0.59 | 0.05 | 0.31 |
| RX sheet (this work) | 0.60 | 0.06 | 0.34 |
| CWSR tubing [17] | 0.58 | 0.10 | 0.32 |

The tensile properties of the Zircaloy-4 sheet used in this study are shown in Table 2 and are described in more detail elsewhere [19]. In comparing the behavior of the two material conditions, we see that the recrystallized (RX) condition exhibits a much higher strain hardening exponent ($n = d\ln\sigma/d\ln\varepsilon$, where $\sigma$ is the stress and $\varepsilon$ is the strain) but lower yield stress values. There is also a significant decrease of the yield stress as the temperature increases from 25° C to 300°C, as is the case for Zircaloy-4 cladding tube [20-22], In both conditions, the texture observed above causes the Zircaloy-4 sheet to be plastically anisotropic such that through-thickness deformation is difficult. Such behavior is apparent from the values of the plastic anisotropy parameter R' ($R' = \varepsilon_{width}/\varepsilon_{thickness}$, where $\varepsilon_{width}$ and $\varepsilon_{thickness}$ are the width and thickness strains during uniform deformation in a tensile test); for the conditions listed in Table 2, R' is in the range of 1.6 to 5.2.

Table 2. Tensile Parameters of Zircaloy-4 sheet in either the recrystallized (RX) or cold worked and stress-relieved (CWSR) conditions at 25° and 300°C for uniaxial testing in the transverse direction of the sheet [19].

| Condition | $\sigma_Y^{0.2\%}$ (MPa) | n-value | R' | Elongation to Failure (%) |
|---|---|---|---|---|
| RX/25°C | 469 | 0.09 | 5.2 | 29 |
| CWSR/25°C | 573 | 0.01 | 2.2 | 19 |
| RX/300°C | 166 | 0.11 | 2.2 | 29 |
| CWSR/300°C | 318 | 0.03 | 1.6 | 16 |

## 2.2 Hydrogen charging

Hydrogen charging of the Zircaloy-4 sheet was performed by gas charging at 400°C using a Ni "window" whose geometry controlled the geometric shape of the hydride (i.e., blister or continuous layer). The Ni window consisted of a thin film of Ni (≈0.1μm thick) that was vapor deposited onto the specimen gauge section with the following geometries: (a) a 2 mm circle, (b) a 3 mm circle (for most of this study), and (c) a continuous layer over the whole gauge section. A short time period prior to vapor deposition, the surface of Zircaloy was cleaned using the ASTM procedure (G2-88) to remove the small oxide layer that is always present in Zr exposed to atmosphere. Uncoated regions of the Zircaloy quickly reformed the small oxide layer prior to exposure to the hydrogen/argon gas at the 400°C, inhibiting the diffusion of hydrogen and

restricting the hydride formation to regions below/near to the Ni coating. As described in detail elsewhere [23], hydrogen charging was performed at 400°C by exposing the coated specimen to a gas mixture of 12.5%$H_2$/argon at one atmosphere pressure and for charging times ranging from 30 s to 30 min. For a given material, it was observed that the depth of the blister was a linear function of the charging time. For the range of charging times used, cross-section metallography showed that the blister diameter corresponded to the Ni coating diameter. In addition, some hydrogen diffused throughout the sheet thickness to form discrete hydrides in the "substrate" region beneath the hydride blister. The resulting hydride distribution is illustrated schematically in Figure 1b with *l* being the blister width (2 or 3 mm) and *d* the blister depth.

## 2.3 Mechanical Testing

In-service loading of Zircaloy cladding tubes usually occurs under multiaxial tension with the maximum principal stress oriented in the hoop direction of the tube. Based on earlier studies [21], we have simulated such loading with a double edge notched tensile specimen, Figure 1a, designed to introduce a biaxial stress state in the specimen center such that near plane-strain tension is achieved (i.e., the minor strain component in the plane of the sheet is near zero). In the present study, 25.4 mm wide specimens (about 76mm long) with two 4.75 mm diameter notches, each of which was 6.35 mm deep, were tested. The resulting biaxial state of stress in the center of the specimen limits strain in the transverse direction of the specimen and induces the material near its center to a near plane-strain deformation path. Failure occurred in the specimen center, where a near plane-strain condition is met, and where the hydride blister was located.

The mechanical testing was performed at an approximate strain rate of $10^{-3}$ $s^{-1}$. In addition, the orientation of the tensile axis was chosen to be in the long transverse direction of the sheet (normal to the rolling direction) in order to obtain deformation behavior similar to that of unirradiated Zircaloy-4 cladding when tested in the hoop direction.

As will be shown later, the hydride blisters fractured at or shortly after yielding within the ductile substrate. In order to determine failure strains of the substrate material beneath the blister, we measured the *local* fracture strain $(\varepsilon_{frac})_{local}$ near, but not at, the fracture surface. After measurement of the initial specimen thickness, cross-section metallography of the fractured specimen was used to determine the specimen thickness at a location approx. 0.5 mm displaced from the fracture surface (to avoid a localized thickness reduction due to crack growth). Using this procedure, we calculated a local thickness strain that we interpret as that strain level at the onset of crack growth. This thickness strain value was then converted into a local failure strain $(\varepsilon_{frac})_{local}$ value by knowing the ratio of minor $(\varepsilon_2)_{blister}$ and major $(\varepsilon_1)_{blister}$ strains within the substrate beneath the blister (measured from the deformation of the circular Ni coating as in the first procedure) and using conservation of the volume. Thus,

$$(\varepsilon_{frac})_{local} = \frac{-\varepsilon_3}{1+\frac{(\varepsilon_2)_{blister}}{(\varepsilon_1)_{blister}}} \qquad (1)$$

For the case in which specimens were hydrided across the entire gauge length (a hydride rim), a microhardness indentation gridding procedure was used to determine the ratio $\varepsilon_2/\varepsilon_1$ on a local basis as done previously [21] .

## 3. RESULTS AND DISCUSSION

### 3.1 Hydride Microstructure

As a result of the hydrogen charging procedure, the blisters were defined by the formation of a solid hydride to a near-uniform depth beneath the Ni coating, as is shown in Figure 2. In the present study, blisters with primarily a 3 mm diameter were formed with depths ranging from 5 to 250 μm. Based on previous studies [24, 25], we believe that the hydride that forms during charging is the δ-phase with a composition range from $ZrH_{1.64}$ to $ZrH_{1.96}$, but no direct confirmation was made. In our case, the kinetics of the blister formation suggest that once a very thin layer of δ-phase forms just below the Ni coating, subsequent hydrogen ingress tends primarily to cause further growth of the δ-phase.

In addition to the formation of a solid hydride blister, some of the hydrogen also forms individual hydride precipitates in the substrate below the hydride blister. As shown in Figure 2a, these hydride precipitates typically have a major dimension on the scale of 100 μm in the CWSR condition and tend to be aligned in the plane of the sheet, similar to the circumferential hydride microstructures in Zircaloy cladding tube. In contrast, the hydrides within the substrate in the RX material appear somewhat smaller (≈25 μm maximum dimension) but tend to have a stronger radial component to their orientation. The hydrogen contents in the ligament below the blister were measured as a function of blister thickness for both RX and CWSR conditions. Results from six different conditions (hydride depths ranging form 50 to 175 μm) show that the H content within the ligament increases from approximately 300 wt. ppm for the 50 μm blister depth to approximately 400 wt. ppm within the ligament below blisters with depth >100 μm.

In summary, the resulting microstructure, shown in Figure 2, consists of a combination of a hydrided substrate residing beneath a solid hydride blister whose width corresponds to the Ni coating dimension (typically 3 mm diameter) and whose depth is controlled by the charging time at $400^0$C (and, to some extent, by the time at the $300^0$C test temperature). It is useful to compare the microstructure shown in Figure 2a (the CWSR case) to that formed during service operation in *irradiated* Zircaloy-4 cladding. For example, Figure 3, which is based on high burn-up Zircaloy cladding, shows a solid hydride layer with a depth ~50 μm as well as the presence of a concentration of discrete, circumferential hydride precipitates. A comparison of Figures 2 and 3 shows that the morphology (shape, aspect ratio, orientation) of the hydrides in the substrate under the model blisters in this study is similar to that observed in the material hydrided in service; this irradiated cladding appears to have a higher density of hydride particles in the substrate beneath the hydride layer.

### 3.2 Effect of Blister Depth on Sheet Failure

Previous research has shown that the thickness of a continuous hydride rim has a strong influence on the failure of Zircaloy-4 cladding; specifically, increasing the thickness of the hydride rim decreases the ductility of the cladding [13, 26]. A similar effect is observed for the case of hydride blisters. The presence of the brittle blister causes the initiation of a crack that propagates to the depth of the blister, as described below. Failure of the sheet is then controlled by fracture of the ductile substrate beneath the blister, which fails at various strain levels, depending on the depth of the blister.

Based on the local fracture strain values, Figure 4 shows that ductility of the Zircaloy-4 sheet containing 3 mm blisters initially decreases rapidly with increasing hydride blister depth for both material conditions and at $300^0$C as well as $25^0$C. For all testing conditions, the rapid decrease in failure strain with increasing blister depth persists to about 100 μm depth. While there is little ductility (2-5%) beyond this value at $25^0$C, moderate ductility (7 to 10% fracture strain for the cold worked material and 10 to 15% for recrystallized condition) is retained at $300^0$C, even for blisters of depths > 200 microns. It is significant that our far-field ductility-values, $(\varepsilon_{frac})_{far}$, as measured over the scale of the 3 mm blister behave in a nearly identical manner to the local fracture strain values shown in Figure 4. Both the dependence of fracture strain on blister depth and the absolute magnitude of the fracture strain values are roughly identical between the two fracture strain procedures.

In addition to the depth of the blister, fracture of the sheet is also sensitive to temperature. Figure 4 also shows that, for a given blister depth, the material is significantly more ductile at 300°C than at 25°C. Although both the CWSR and the RX conditions show similar behavior at 25°C, the recrystallized condition shows significantly more ductility than the CWSR material at 300°C. This result is somewhat surprising since the RX condition contains a higher level of radial hydrides (known to promote fracture) within the substrate, as shown in Figure 2.

The influence of blister size, as opposed to blister depth, is illustrated in Figure 5, which shows that specimens with 2 mm diameter blisters exhibit approximately the same ductility as do 3 mm diameter blisters. Although no blister with a 2 mm diameter was tested at 300°C, we believe that the behavior at 300°C is similar to room temperature regarding the blister size. Therefore, these results indicate that the *ductility of specimens with hydride blisters depends mainly on the depth of the blister and not on its diameter* (either 2 or 3mm).

Figure 5 also compares the influence of blisters with that of a continuous hydride rim on fracture. In both the blister and rim cases, the ductility decreases rapidly with increasing hydride layer depth up to depths of ~ 100 μm. However, the decrease in fracture strain is more severe when the hydride layer is present in the form of a rim, especially at small blister/rim depths. For example, the fracture strain for a specimen with a 3-mm diameter and a 20 μm thick blister is about 0.24, while it is only about 0.12 for a specimen with a 20 μm continuous layer of hydride. Similar results, although not as complete as those in Figure 5, have been obtained for specimens tested at 300°C. Thus, the ductility of a material containing a continuous hydride rim is *less* than that of a material containing blisters of the same depth; this effect is most pronounced at small blister/rim depths.

Comparing to previous studies performed on tubing [13, 26], the fracture strains obtained in this study with *sheet material* containing a hydride rim are very similar to those obtained previously on *tubing* with hydride rim. This supports our contention that the behavior of sheet material is a good model for that of tubing material with similar texture.

Finally, we note that, along with increased fracture strain at small blister depths, there is also a change in strain path. For thick blisters, the lateral constraint from the blister and the presence of cracks forces the Zircaloy substrate to a condition close to plane-strain deformation (i.e., referring to Figure 1, $\varepsilon_{yy} \approx 0$). Alternatively, the lack of transverse constraint from thin blisters as well as the high R-value of the substrate sheet metal results in a significantly larger minor strain in specimens with thin blisters. This change in strain path likely contributes to the observed increase in fracture strain at thicknesses below 50 microns (Figures 4 and 5). We offer this speculation on the basis that fracture of sheet metal usually depends on a critical thickness strain criterion [27]. Thus, any change in strain path in which the minor strain increases requires a compensating increase in major strain to achieve the critical thickness strain. In short, sheet metal ductility increases as the strain path deviates from plane-strain tension.

### 3.3 Mode of Failure: Fracture Profiles

While failure of the Zircaloy sheet initiates with cracking of the blisters both at 25° C and at 300°C, the mode of fracture of the substrate material (which determines the ductility of the hydrided sheet) depends on temperature. Figure 6 shows that the fracture profiles differ significantly between specimens tested at 25°C and 300°C. Independent of blister depth, the fracture profiles at 25°C are characterized by crack growth in the substrate along a path roughly *normal to the specimen surface* and therefore also normal to the maximum principal stress. Given the presence of 300-400 wt ppm hydrogen and the resulting hydride precipitates in the substrate, crack growth appears to result from damage accumulation within the substrate in the form of voids initiated by cracked hydrides, as shown in Figure 7. Thus, at 25°C, failure of the Zircaloy substrate occurs as a result of a crack growth process on a plane normal to the maximum principal stress and involving the growth and coalescence of voids formed by the cracked hydride precipitates.

In contrast to room temperature behavior, fracture of the substrate at $300^0$C substrate occurs on a macroscopic plane inclined at ≈ 45° through the thickness, as also shown in Figure 6c and 6d. Such behavior suggests an alternate failure mode to crack growth. Specifically, we believe that the through-thickness shear failure evident in Figure 6c and 6d is a result of a deformation localization process on a plane of high shear stress, in the manner of localized necking of sheet metal [27, 28]. The pronounced crack blunting at 300°C indicates that cracks initiating within the blister are arrested by a very ductile, crack-resistant substrate. Significantly, the cracks appear to be more blunted in the RX condition than in the CWSR condition. This behavior is consistent with the increased ductility of the RX condition (see Figure 4), despite the presence of some radial hydrides in the RX material.

### 3.4 Fracture of Hydride Blisters

The failure behavior of Zircaloy sheet with hydride blisters (and, we believe, Zircaloy cladding tubes with hydride blisters) can be understood as a sequential process of crack initiation within the hydride blister and the subsequent failure of the substrate material beneath the blister. In the present study, both acoustic emission results at room temperature and tests performed at temperatures up to $400^0$C and interrupted at small strains ($\varepsilon \leq 0.02$) show the blister cracks at small

plastic strains ($\varepsilon \leq 0.02$) within the substrate beneath the blister. In all cases, cross-section metallography shows the cracks are oriented normal to the blister surface and extend through its depth, consistent with their brittle behavior; i.e. the cracks arrest at the ductile substrate. Thus, we conclude that the hydride blisters are brittle at temperatures $\leq 400°$ C. Because the blisters are not only brittle but also reside on a ductile substrate, multiple cracks (all of which extend the width of the blister) form during deformation of the sheet, as illustrated in Figure 9. The crack spacing decreases roughly linearly with blister depth. A detailed analysis of the fracture behavior of hydride blisters is described elsewhere [28].

## 4. FRACTURE MECHANICS ANALYSIS

The results described above indicate that the fracture behavior is sensitive to blister depth as well as temperature. In all cases, the hydride blisters crack at small strains and fracture of the sheet is controlled by failure of the ductile substrate beneath the blister. While substrate failure at $300^0$C appears to result from a shear instability, room temperature fracture has the characteristics of crack growth (i.e., fracture along a plane normal to $\sigma_1$ accompanied by comparatively little local necking). As described elsewhere [23,28], it is possible to use an elastic-plastic analysis to predict fracture *strains* necessary to propagate the crack within a blister of a given depth and to cause sheet fracture.

We assume that the hydride blister/rim of depth *a* is equivalent to a crack of the same initial depth *a* (a consideration of the presence of parallel cracks and crack-tip shielding indicates that the single crack assumption is reasonable [23,28]) and that the geometries for both hydride rim and blister configurations correspond to a semi-infinite surface crack or a semi-elliptical surface crack, respectively. In both cases, the cracks reside in a sheet of finite thickness, and we assume plane-stress conditions through the thickness. Because of the large amount of plastic yielding that occur during crack growth, the J-integral procedure is used, as is described below.

In order to account for plasticity, the material is assumed to follow the Ramberg-Osgood equation:

$$\frac{\varepsilon}{\varepsilon_0} = \frac{\sigma}{\sigma_0} + \alpha\left(\frac{\sigma}{\sigma_0}\right)^{n'} \qquad (2)$$

where $\sigma_0$ is the yield stress, $\varepsilon_0 = \frac{\sigma_0}{E}$, $E$ is the elastic modulus, $n'$ is the inverse of the strain-hardening exponent ($n' = \frac{1}{n}$), and $\alpha = \frac{{\sigma_0}^{n'-1}E}{k^{n'}}$ and where k is given by the equation:

$$\sigma_{eq} = k(\bar{\varepsilon}_N)^n \qquad (3)$$

where $\sigma_{eq}$ is the equivalent stress and $\varepsilon_N$ is the void nucleation strain.

Therefore, the plastic strain at the crack tip will be equal to:

$$\varepsilon_n^p = \alpha \frac{\sigma_0}{E}\left(\frac{\sigma_n}{\sigma_0}\right)^{n'} \qquad (4)$$

where $\sigma_n$ is the net-section stress, $\sigma_n = \dfrac{\sigma}{1 - a/t}$.

where t is the thickness. Fracture occurs when the driving force for the crack propagation, $J(a_e, \sigma)$, reaches the critical value $J_c$; and so the condition for crack propagation can be expressed as

$$J(a_e, \sigma) = J_c = \frac{K_c^{\,2}}{E} \qquad (5)$$

where $K_c$ is the plane-stress fracture toughness of the sheet. The J-integral may be separated into elastic $J_e(a_e, \sigma)$ and plastic $J_p(a_e, \sigma)$ components and then is equal to:

$$J(a_e, \sigma) = J_e(a_e, \sigma) + J_p(a_e, \sigma) = J_e(a_e, \sigma)\left[1 + \alpha\left(\frac{\sigma_n}{\sigma_0}\right)^{n'-1}\right] \qquad (6)$$

where $J_e(a_e, \sigma) = \dfrac{K_e^{\,2}}{E}$ for plane-stress conditions. Substituting (4) into Equation (2) leads to the following relationship for the fracture plastic strain:

$$\varepsilon_n^p = \alpha \frac{\sigma_0}{E}\left\{\frac{1}{\alpha}\left(\frac{K_c^{\,2}}{K_e^{\,2}} - 1\right)\right\}^{\frac{n'}{n'-1}} \qquad (7)$$

Equation 12 permits us to predict the fracture strain provided that we know the stress-intensity factor $K_e$ for the crack geometries. In all cases, we apply the "plastic zone correction" procedure by considering a hypothetical crack of length $a_e = a + r_{0\sigma}$, where $r_{0\sigma}$ is half of the plastic zone size in plane-stress conditions or

$$r_{0\sigma} = \frac{1}{2\pi}\left(\frac{K_e}{\sigma_0}\right)^2 \qquad (8)$$

The plastic zone $2r_{o\sigma}$ is obtained by first calculating $K_e$ with $a_e$=a; then $K_e$ is recalculated using $a_e = a + r_{0\sigma}$.

In order to determine the stress intensity parameter for the case of the cracked hydride blisters, the crack geometry correction factor for a semi-elliptical crack in a strip of finite thickness was employed [36]. For the case of the continuous hydride rim, the correction factor was that for a semi-infinite surface crack in a strip of finite thickness. These correction factors are based on the presence of a single crack in the material.

In order to apply the crack-growth analysis described, the fracture toughness, $K_c$, must be known. For Zircaloy-4 cladding tubes, previous studies show $K_c$-values to depend on H content and temperature. $K_c$-values in the range of 120-150 MPa.m$^{1/2}$ are common for unhydrided Zircaloy-4 at

both room temperature and 300°C. At room temperature, Grigoriev et. al. [29] found $K_c$-values about 104 MPa.m$^{1/2}$ for H contents 400-600 wt. ppm (assuming the following relationship: $K_c = \sqrt{J_{max} E}$, with $J_{max}$ the $J_I$-integral for the maximum load point, and E the elastic modulus). Based on data from Huang [30], Kuroda et. al. assumed $K_{IC}$-values of 73 MPa.m$^{1/2}$ in their fracture mechanics analysis of hydrided Zircaloy-4 cladding at room temperature[31]. At 300°C, the H content does not appear to influence the fracture toughness [29], in which case $K_c \cong$ 120-150 MPa.m$^{1/2}$ [32]; Grigoriev et. al. report a $J_{max}$-value that indicates $K_c \cong$ 117 MP.m$^{1/2}$ at 300$^0$C for 400 wt. ppm H [29] . In addition, the nominal stress $\sigma$ was calculated using Hill's original yield function for plane-strain condition and the constitutive stress-strain relation expressed in Equation 6 with the equivalent strain being given by Equation 4. An iterative calculation was then made to obtain the fracture strain $\varepsilon_n^p$. The material properties used in the analysis for both temperatures and materials (CWSR and RX) are given in Table 3.

Table 3. Material properties used in the fracture mechanics analysis.

| Property | CWSR | | RX | |
|---|---|---|---|---|
| | 25°C | 300°C | 25°C | 300°C |
| n | 0.01 | 0.025 | 0.087 | 0.112 |
| n' | 100 | 40 | 11.5 | 8.9 |
| E (GPa) | 100 | 75 | 100 | 75 |
| $\sigma_0$ (MPa) | 573 | 318 | 469 | 166 |

Figure 9 shows the comparison between the fracture mechanics predictions and the observed dependences of fracture strain on blister/rim depth. As shown in Figure 9a, the agreement between experimental results and crack growth predictions are quite good assuming $K_c$ = 70 MPa.m$^{1/2}$, which is a value close to that (73 MPa.m$^{1/2}$) assumed by Kuroda et. al. [31]. Bearing in mind that our substrate material contains 300-400 wt ppm hydrogen, the 70 MPa-value is similar but somewhat less than that (90 MPa.m$^{1/2}$) observed by Grigoriev et. al. [39]. In addition, close inspection of Figure 9a shows that the calculated fracture strains for the two blister diameters (2mm and 3mm) are superimposed on each other. This supports our earlier conclusion, based on experimental observations, that the blister diameter (2 or 3 mm) has no significant effect on the failure of Zircaloy-4.

Figure 9b shows that the influence of the continuous hydride rim on fracture can also be predicted by our crack growth analysis, also on the basis of $K_c \cong$ 70 MPa.m$^{1/2}$. Reasonable agreement between the predicted and observed dependences is obtained. The predicted fracture mechanics results also confirm the earlier experimental observation that, compared to a hydride blister, a continuous hydride rim is more deleterious to ductility at a given hydride depth.

For the case of the recrystallized materials, the crack growth analysis fits experimental observations, Figure 9c, using a $K_c$-value between 100 and 150 MPa.m$^{1/2}$. While somewhat surprising, the increased $K_c$-value of the RX material is consistent with its lower flow stress and increased tensile ductility. For example, an unhydrided plane strain specimen was tested as well as a sister sample hydrided in the form of discrete hydride precipitates through the whole thickness below the Ni coating (no solid hydride blister was present) at a H concentration similar to that of the

hydrided substrates, both at room temperature and in the RX condition. Very similar average strains were found. Those results show that the tensile ductility of the hydrided substrate is similar to that of the unhydrided material and, importantly, significantly higher in the RX compared to the CWSR condition. Thus, it is reasonable the RX material exhibits more crack growth resistance than the CWSR material.

## 5. DISCUSSION

The experimental results presented here represent a reasonably complete picture of the behavior of Zircaloy sheet containing blisters at room temperature and at 300 C. The model developed in the previous section accounts well for the fracture strains observed at 25 C, but at 300 C, a different failure process is operative, and the model is no longer applicable. Earlier experimental observations, Figure 6, indicated a transition in failure mode from crack growth at room temperature to shear instability at $300^0$C. Such a transition is consistent with our observation that the strains to nucleate voids at cracked hydride particles increase markedly with increasing temperature [28]. It is also consistent with the observation of a much reduced level of hydrogen embrittlement in Zircaloy-4 at $350^0$C [7]. Thus, we expect a significant increase in fracture strain within the crack-tip process zone and therefore higher fracture toughness at $300^0$C, consistent with experimental observations [29]. As shown in Figure 9d, the elevated values of the fracture toughness result in a significantly over-prediction of the experimentally observed fracture strains. Thus, we conclude that our unirradiated Zircaloy-4 containing hydride blisters does not fail by crack growth, but rather by a competing mechanism: a deformation localization process in which failure occurs by shear localization. An alternate failure model should be used to predict the experimental data at 300ºC, but an adequate analysis is not currently available.

The current experiments were undertaken as a model study to identify the influence of model hydride blisters on Zircaloy ductility. As such, this model does not reproduce exactly the failure conditions of hydrided cladding in the reactor. In addition to the other parameters present in the reactor environment that also influence failure, such as radiation damage, there are additional factors that make the present tests different. When blisters form in fuel cladding, they often do so on top of an existing hydride rim, which may or may not be partially dissolved. Such a configuration should have a more severe impact on ductility than the isolated blister configuration used in our work.

Because of the above reasons, the absolute values of ductility do not necessarily correspond to the ductility that would be exhibited by Zircaloy cladding in a reactor. Nevertheless, this study does provide a systematic identification of the effects of hydride blisters on ductility under deformation conditions that are similar to those that would be expected during a reactivity initiated accident, especially if little friction exists between fuel and cladding. In particular, the temperature dependence of the effects should also be useful for understanding in-reactor behavior. For the case where fuel/cladding friction is very high, equal biaxial behavior should be prevalent and studies are ongoing to determine Zircaloy ductility under those conditions.

## 6. CONCLUSIONS

Both cold-worked and stress-relieved (CWSR) and recrystallized (RX) Zircaloy-4 sheet specimens were hydrided to form either 2 mm or 3 mm solid hydride blisters of controlled depths residing on a substrate that contains ~300-400 wt. ppm hydrogen in the form of discrete hydride particles. Limited tests were also performed on material with a continuous hydride layer. The fracture behavior of these materials were studied (primarily at 25° and 300°C) using double edge notched tensile specimens designed to induce near plane-strain deformation. The main conclusions are as follows:

1. In all cases, the hydride blisters are brittle even at $400^0$C. A population of cracks forms and propagates through the blisters soon after the yielding of the plastic substrate beneath the hydride blister. The crack spacing in the blisters decreases with blister thickness.
2. Fracture of the sheet is controlled by the crack growth resistance of the substrate, such that the fracture strains decreases with increasing hydride blister/layer depth to levels of about 100 μm deep, above which the ductility remained constant. At $300^0$C, both CWSR and RX Zircaloy-4 retain moderate ductility (7-10% fracture strain for CWSR and 10-15% for the RX condition), even for blister depths > 200 micron, which is close to one third of the sheet thickness.
3. The material is significantly more ductile at $300^0$C than at room temperature. Also, the sheet is somewhat more ductile if the hydride is present as a blister rather than as a continuous layer. Blisters with 2 mm or 3 mm diameter have the same effect on sheet ductility.
4. An examination of the fracture profiles indicates a transition in failure mode within the substrate from crack growth on a plane normal to the maximum principal stress at $25^0$C to a shear instability process on an inclined plane at $300^0$ and $400^0$C. At room temperature, the cracks that initiate within the hydride blisters (as well as in the continuous layers) propagate in a manner that can be predicted using elastic-plastic fracture mechanics. The observed fracture strains and their dependence on hydride blister depth can be well predicted using this model.

## ACKNOWLEDGMENTS

We would like to thank Dave Green at Penn State for many technical discussions and Ralph Meyer at the NRC for his continued encouragement. This research has been supported by the Fermi Consortium at Penn State (ONP) and by the Southwest Research Institute (KSC).

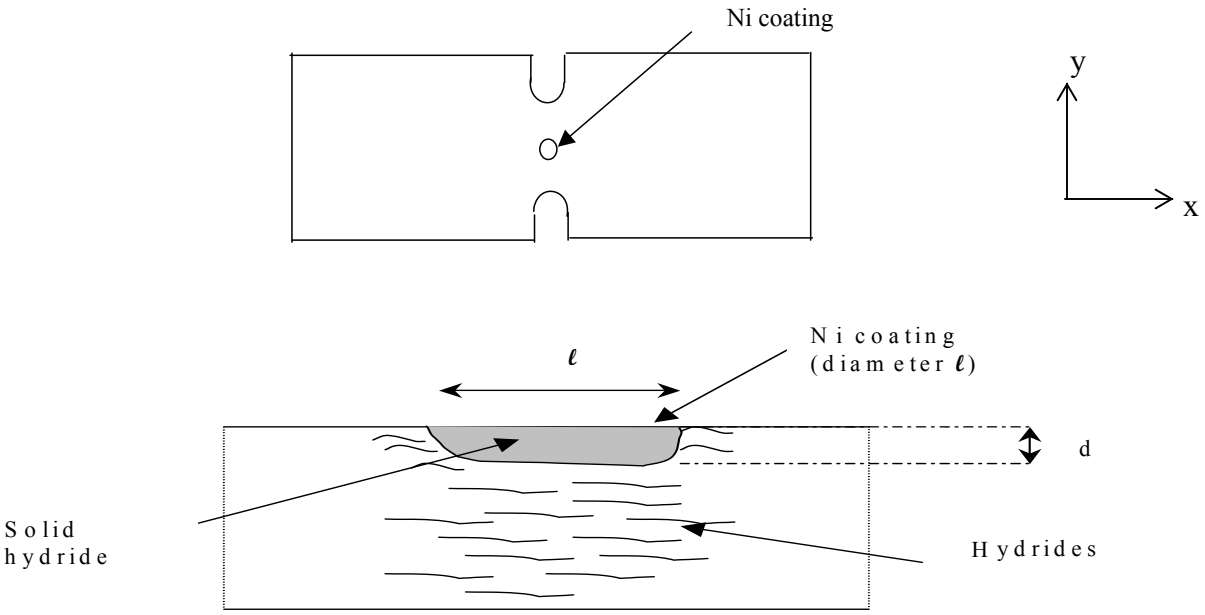


Figure 1. A schematic of (a) a double edge notched tensile specimen with a Ni coating/hydride blister in its center and (b) hydride blister made by hydrogen charging through a Ni coating with diameter *l*. The y direction is parallel with the rolling direction.

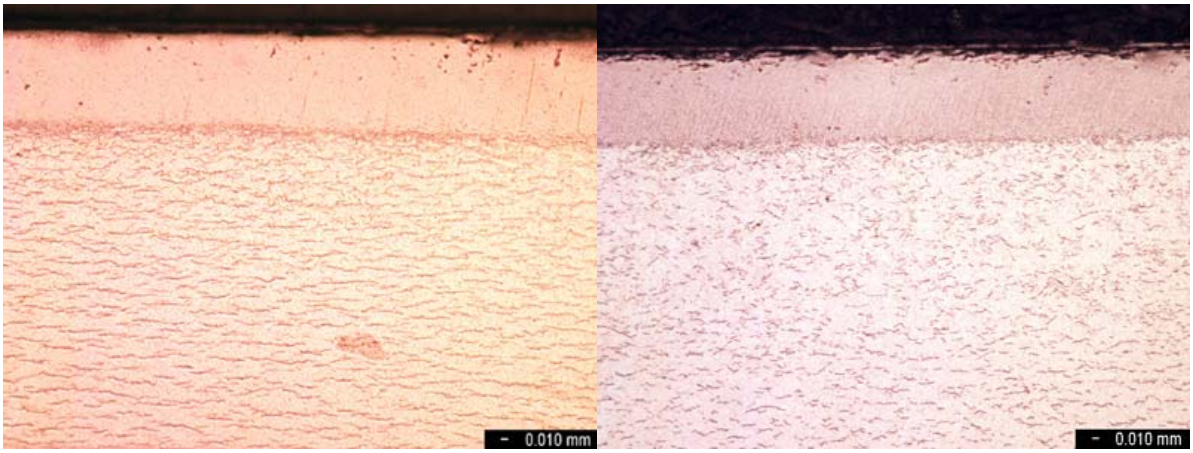


(a) (b)

Figure 2. Light micrographs of a transverse section of Zircaloy-4 sheet showing hydride blister and discrete hydride precipitates within the substrate beneath the blister in (a): CWSR specimen and (b): RX specimen.

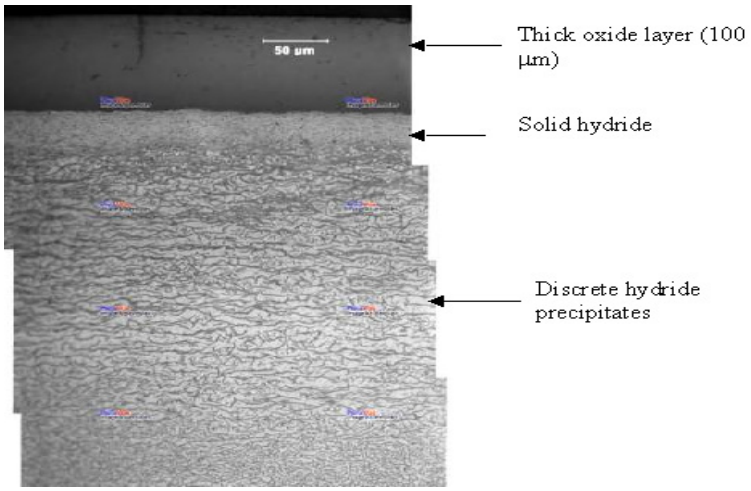


Figure 3. A light micrograph showing a hydride layer and associated hydrides in the substrate beneath the layer in irradiated Zircaloy-4 cladding tube (average fuel burnup of 67 GWd/t and fast fluence of $1.3 \times 10^{22}$ n/cm$^2$).

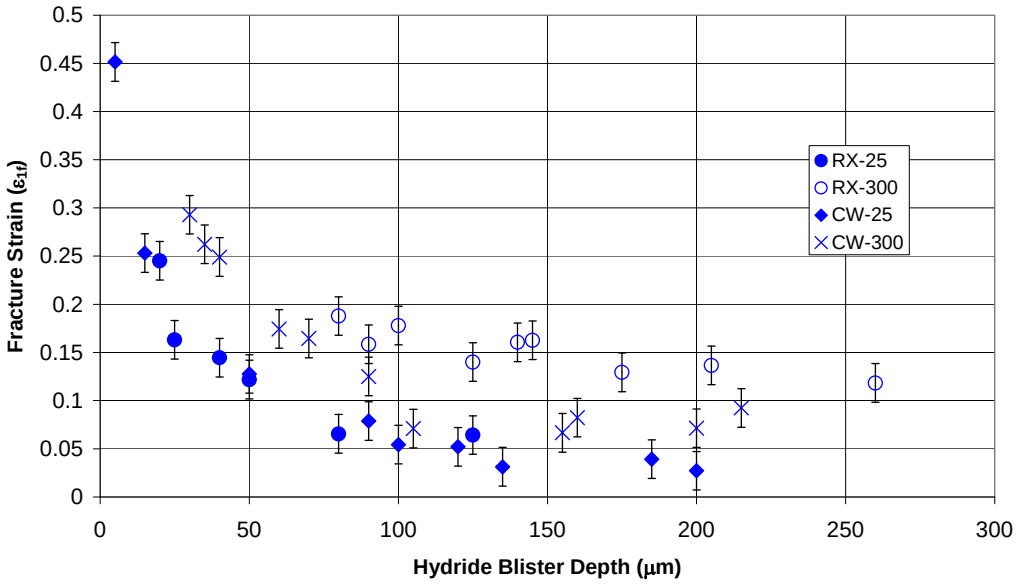


Figure 4. Local fracture strain versus hydride blister thickness for both cold worked and stress relieved (CWSR) and recrystallized (RX) Zircaloy-4 sheet tested at either $25^0$C or $300^0$C. All data are for 3 mm blisters.

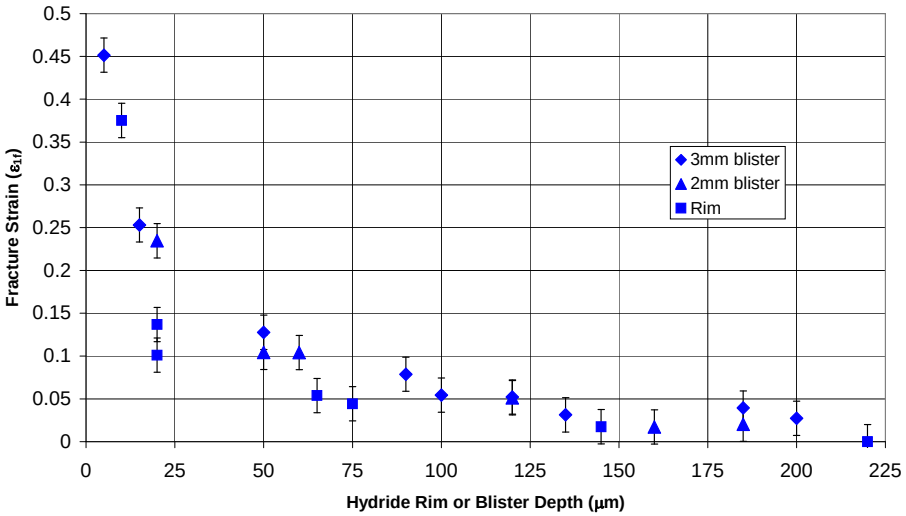


Figure 5. Local fracture strain versus blister or rim depth for either 3 mm or 2 mm diameter hydride blisters or a continuous rim of hydrides ($25^0$ C).

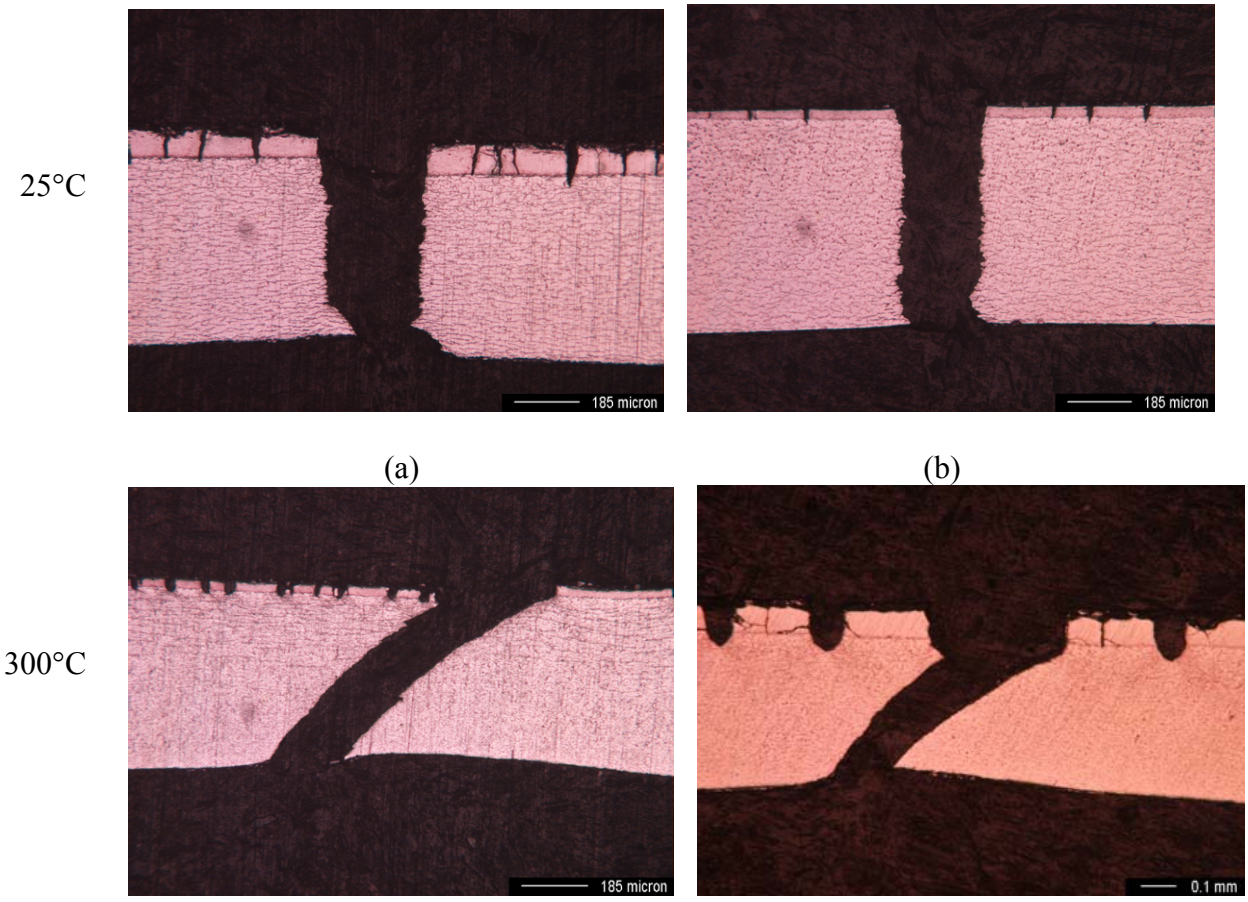


Figure 6. Fracture profiles of (a) CWSR sheet with a 100 μm blister, (b) RX with 40 μm blister, (c) CWSR with 35 μm blister, and (d) RX with 80 μm blister. Test temperatures are indicated.

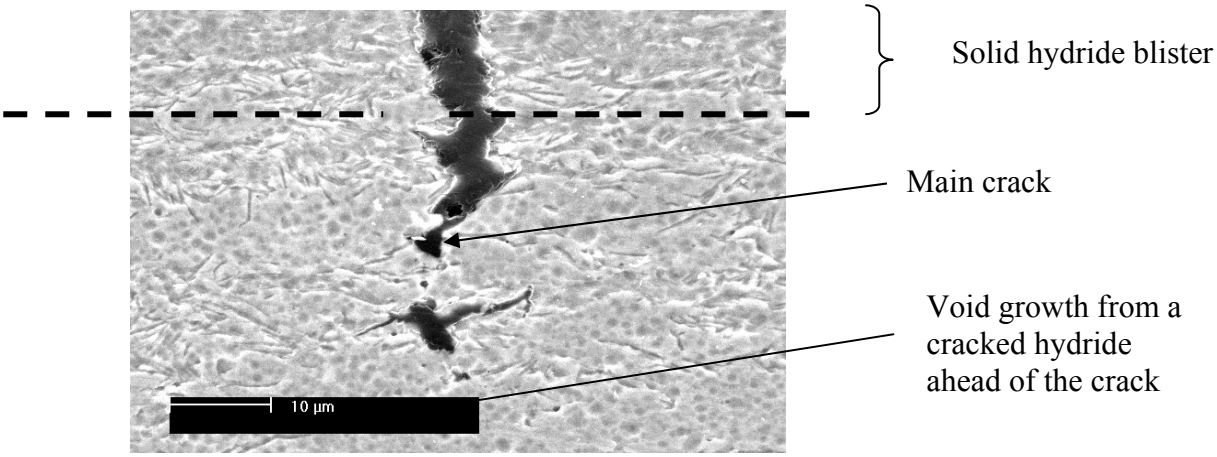


Figure 7. A light micrograph showing fractured hydrides and void nucleation near the tip of a crack beneath a 200 µm blister in CWSR Zircaloy-4 deformed at room temperature

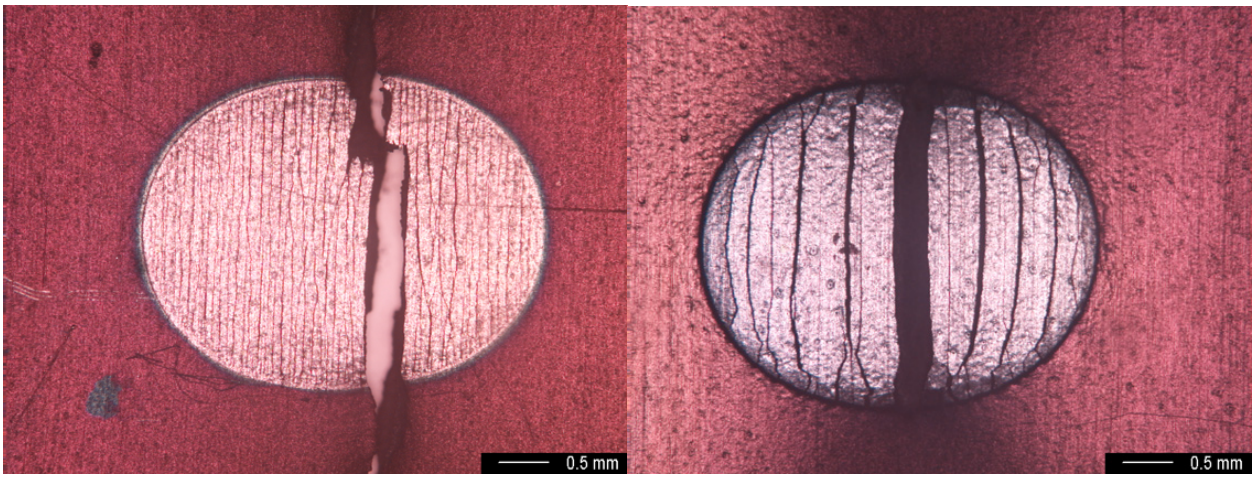


(a) (b)

Figure 8. Macrographs of cracked blisters in CWSR material failed at (a) $25^0$C and with a 50 µm deep blister and (b) $300^0$C with a 105 µm deep blister.

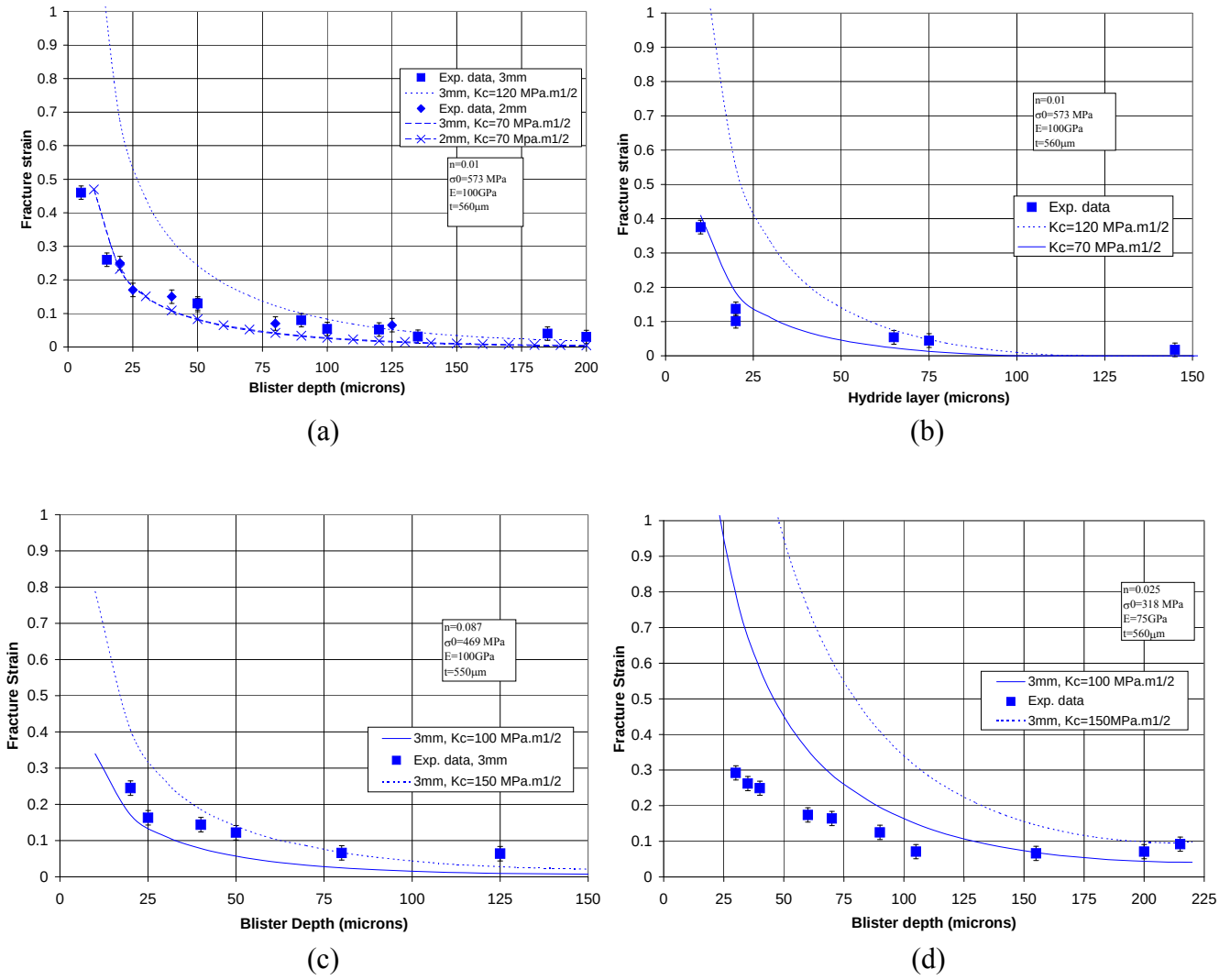


Figure 9. The dependence of observed and predicted fracture strain strains for (a) CWSR Zircaloy-4 with hydride blisters at $25^0$C, (b) CWSR Zircaloy-4 with a hydride rim at $25^0$C, (c) RX Zircaloy-4 with blisters at $25^0$C, and (d) CWSR material with hydride blisters at $300^0$C.

## REFERENCES


[1] C. Lemaignan and A. T. Motta, "Zirconium in Nuclear Applications," in *Nuclear Materials*, vol. 10B, B.R.T.Frost, Ed. New York: VCH, 1994, pp. 1-52.

[2] A. M. Garde, G. P. Smith, and R. C. Pirek, in *11th International Symposium on Zr in the Nuclear Industry*, vol. STP 1295. American Society for Testing and Materials, West Conshohocken, PA, (2002) pp.407-430.

[3] C. E. Coleman and D. Hardie, *J. Less-Common Metals*, **2**, 1966, 168-185.

[4] C. E. Ells, *J. Nucl. Mater.*, **28**, 1968, 129-151.

[5] L. A. Simpson, *Metall. Trans.A,*, **12A**, 1981, 2113-2124.

[6] S. Yamanaka, M. Kuroda, D. Setoyama, M. Uno, K. Takeda, F. Nagase, and H. Uetsuka, *J. Alloys and Compounds*, **330-332**, 2002, 400-403.

[7] J. B. Bai, C. Prioul, and D. Francois, *Metall. and Mater. Trans.A*, **25A**, 1994, 1185-1197.

[8] F. Prat, M. Grange, J. Besson, and E. Andrieu, *Metall. and Mater. Trans.A,*, **29A**, 1998, 1643-1651.

[9] M. Grange, J. Besson, and E. Andrieu, *Metall. and Mater. Trans.A,*, **31A**, 2000, 679-690.

[10] M. Kuroda, K. Yoshioka, S.Yamanaka, H. Anada, F. Nagase, and H. Uetsuka, *J. Nucl. Sci. Tech.*, **37**, 2000, 670-675.

[11] M. Kuroda, S. Yamanaka, D. Setoyama, M. Uno, K. Takeda, H. Anada, F. Nagase, and H. Uetsuka, *J. Alloys Compounds*, **330-332**, 2002, 404-407.

[12] S. I. Hong, K. W. Lee, and K. T. Kim, *J. Nucl. Mater.*, **303**, 2002, 169-176.

[13] Daum, R. S., S. Majumdar, M. C. Billone, D. W. Bates*, D. A. Koss and A. T. Motta, 13th International Symp. on *Zirconium in the Nuclear Industry*, ASTM STP 1423, (2002) pp. 696-713.

[14] F. Yunchang and D. A. Koss, *Metallurgical Transactions A*, **16A**, 1985, 675-681.

[15] R. O. Meyer, R. K. McCardell, H. M. Chung, D. J. Diamond, and H. H. Scott, *Nuclear Safety*, **37**, 1996, 872-387.

[16] J. J. Kearns and C. R. Woods, *J. Nucl. Mater.*, **20**, 1966, 241.

[17] P. Delobelle, P. Robinet, P. Bouffioux, P. Greyer, and I. LePichon, 11th International Symposium on Zr in the Nuclear Industry, 1996; ASTM STP 1295; Garmisch-Partenkirchen, 373-393.

[18] E. Tenckhoff, *Deformation Mechanisms, Texture and Anisotropy in Zirconium and Zirconium Alloys*, vol. 966. Philadelphia: ASTM, 1988.

[19] O. N. Pierron, D. A. Koss, and A. T. Motta, *accepted for Journal of Nuclear Materials*, 2002.

[20] T. M. Link, "Failure of Zircaloy Cladding under Severe Loading Conditions," M.Sc. thesis; in *Materials*. Penn State Univesrity, University Park, PA; 1997.

[21] T. M. Link, D. A. Koss, and A. T. Motta, *Nuclear Engineering and Design*, **186**, 1998, 379-394.

[22] SCDAP/RELAP5/MOD2, *Code Manual volume 4: MATPRO: "A Library of Materials Properties for Light Water Reactors Accident Analysis", NUREG/CR-5273, EG-2555, chapter 4.9.*, 1990.

[23] O. N. Pierron, "Influence of Hydride Blisters on Failure of Zircaloy-4 Sheet," M.Sc. thesis; in *Materials*. Penn State University, University Park; 2002.

[24] G. E. Fernandez and G. Meyer, *J. Nuc. Mater.*, **279**, 2000, 167.

[25] J. Bloch, I. Jacob, and M. H. Hintz, *Journal of Alloys and Compounds*, **191**, 1993, 179-186.

[26] Daum, R. S., S. Majumdar, H. Tsai, T. S. Bray, D. A. Koss, A. T. Motta and M. C. Billone, *Small Specimen Test Techniques: Fourth Volume*, ASTM STP 1418, M. A. Sokolov, J. D. Landes, and G. E. Lucas, Eds., American Society for Testing and Materials, West Conshohocken, PA, (2002) pp.195-210

[27] K. S. Chan, D. A. Koss, and A. K. Ghosh, *Metallurgical Transactions A*, **15A**, 1984, 323-329.

[28[ O.N.Pierron, D.A.Koss, A.T.Motta and K.S.Chan, submitted to the J. of Nuclear Materials, 2002.

[29] V. Grigoriev, B. Josefsson, and B. Rosborg, 11th ASTM International Symposium on Zr in the Nuclear Industry, 1996; ASTM STP 1295; Garmisch-Partenkirchen, Germany, 431-447.

[30] F. H. Huang, *J. Nucl. Mater.*, **207**, 1993, 103-115.

[31] M. Kuroda, S. Yamanaka, F. Nagase, and H. Uetsuka, *Nucl. Eng. Des.*, **203**, 2001, 185.

[32] Asada, T., Kimoto, H., Chiba, N., and Kasai, Y., 9th Zirconium in the Nuclear Industry, ASTM STP 1132, C.M.Eucken and A.M.Garde eds., Philadelphia 1991, 99-118.